ACS APPLIED MATERIALS & INTERFACES

Research Article

www.acsami.org

Hydrothermal Synthesis of Phosphate-Functionalized Carbon Nanotube-Containing Carbon Composites for Supercapacitors with Highly Stable Performance

Xiaoming Fan, Chang Yu, Zheng Ling, Juan Yang, and Jieshan Qiu*

Carbon Research Laboratory, Liaoning Key Lab for Energy Materials and Chemical Engineering, State Key Lab of Fine Chemicals, School of Chemical Engineering, Dalian University of Technology, Dalian 116024, China

Supporting Information

ABSTRACT: Phosphate-functionalized carbon nanotube (CNT)-containing carbon composites with hierarchical porous structure have been synthesized by a simple soft-template hydrothermal method followed by heat treatment. The resulting carbon composites are characterized by FE-SEM, TEM, TGA, FTIR microspectroscopy, and nitrogen sorption techniques. The electrochemical performance of the carbon composites as electrode materials for supercapacitors is also investigated. The results show that CNTs can be uniformly embedded in the carbon matrix, and the phosphate groups are introduced into the carbon composites successfully. The addition of CNTs with suitable content significantly improves the rate capability of carbon composites in 6 M KOH aqueous solution. Cell voltage window can be extended to 1.2 V when increasing the heat treatment temperature of carbon composites to 800 °C, and the resulting composites exhibit highly stable performance in supercapacitors at high current load of 5 A g^{-1} and wide cell voltage of 1.2 V.

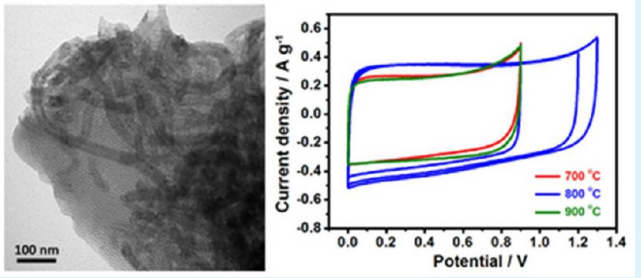

KEYWORDS: *phosphate functionalization, carbon nanotube, fructose, supercapacitor*

1. INTRODUCTION

Carbon materials have received much attention as the electrode materials for supercapacitor energy storage device because of their intriguing properties including low cost, easy availability, nontoxic nature, environmental friendliness, and stability.[1,2] The energy density, power density, and stable charge−discharge performance for supercapacitors are governed by the carbon electrodes to a great degree. The physical and chemical properties of carbon materials are the key factors affecting their electrochemical performance in supercapacitors. Up to now, various strategies for tuning the properties of carbon materials with an aim of further enhancing their electrochemical performance have been developed by optimizing the pore structure,[3,4] introducing heteroatom functional groups[5,6] and coupling with nanocarbons,[7,8] or pseudocapacitive materials.[9,10] Of these strategies available now, heteroatom functionalization with phosphate groups is one of the promising approaches, which can improve the stability of active oxygen-containing groups on carbon materials during the charging and discharging process and widen the operating voltage window for higher energy density.[11] Highly conductive nanocarbons including carbon nanotube, graphene, and carbon onion as additives have been used to improve the resulting conductivity of the carbon electrode materials for supercapacitors. This has been confirmed by the Dai's group, in which nanocarbons such as carbon onion was incorporated in the framework of mesoporous carbons with high electrical conductivity by "brick-and-mortar" approach and the electrochemical performance was further improved.[12] Carbon nanotubes (CNTs) have been widely used for the electrode materials of supercapacitors owing to the excellent properties such as high electrical conductivity and relatively large specific surface area with opened mesoporous structure.[13,14] Making use of CNTs as nanotexturing agent to make carbon composites with "brick-and-mortar" structures where CNTs are embedded in the carbon matrix can help create networks with opened mesoporous structure for ions propagation, which also lead to better electrical conductivity and mechanical stability. Because of this, various CNT/carbon composites including activated CNT/carbon[15] and biopolymer-based CNT/carbon[7] have been fabricated, showing highly stable supercapacitive performance at high rate.

Biomasses and their derivatives are cheap, ubiquitous, and renewable natural resources, which have been widely used to fabricate functional carbon materials by pyrolysis or hydrothermal technologies. Compared with the conventional pyrolysis technology, the hydrothermal approach has been demonstrated to be a powerful technique to convert different types of biomasses to hydrothermal carbon materials (HTCs)

Received: December 10, 2012
Accepted: February 28, 2013
Published: February 28, 2013

Scheme 1. Schematic of the Synthesis of the Samples

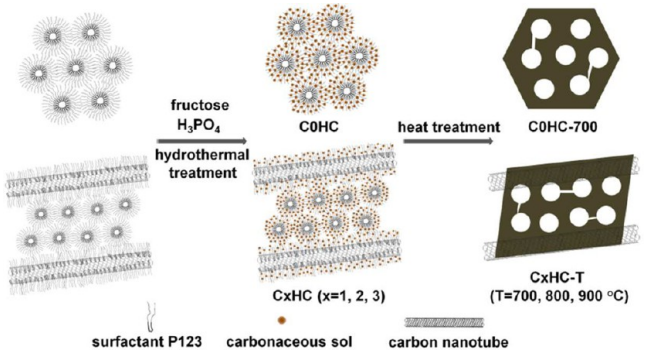

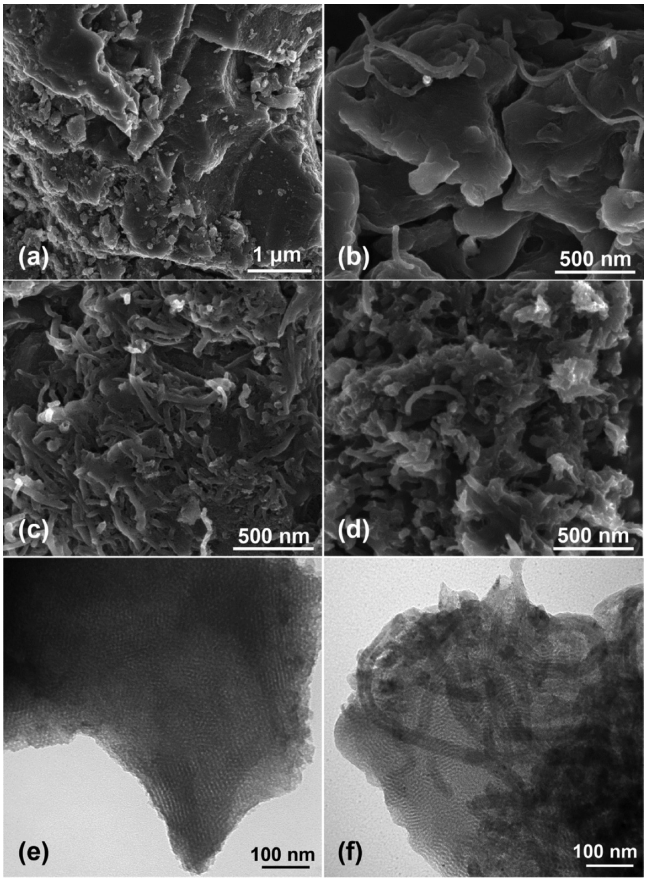

Figure 1. FE-SEM images of (a) C0HC-700, (b) C1HC-700, (c) C2HC-700, (d) C3HC-700, and TEM images of (e) C0HC-700, (f) C2HC-700.

with diversified structures by controlling the liquid-phase reaction environment.[16] Recently, it has been found that ordered mesoporous HTCs can be made by one-pot self-assembled process with triblock copolymer as template.[17] Hydrothermal carbon made from fungi also showed good capability as electrode materials in supercapacitors.[18] Nevertheless, these HTCs usually have relatively small surface area and pore volume, resulting in poor capacitance.[19,20]

In this study, we report on a simple soft-template hydrothermal method with fructose as a carbon source followed by heat treatment, which can produce phosphate-functionalized CNT-containing carbon composites with controlled hierarchical porous structure, and the as-prepared functional carbon

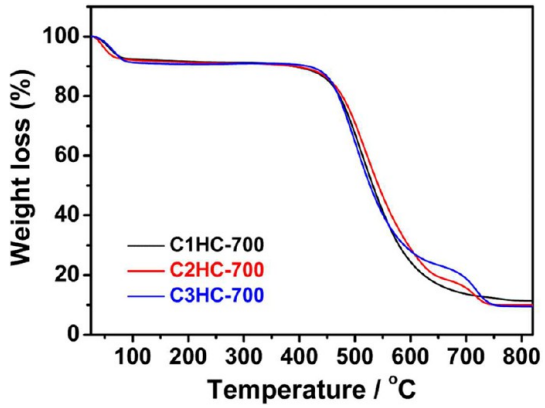

Figure 2. Thermogravimetric profiles of the carbon composites with different CNT contents.

Table 1. Electrical Conductivity Values of the Samples

sample	C0HC-700	C1HC-700	C2HC-700	C3HC-700
electrical conductivity (S m^{-1})	0.02	0.08	1.52	2.11

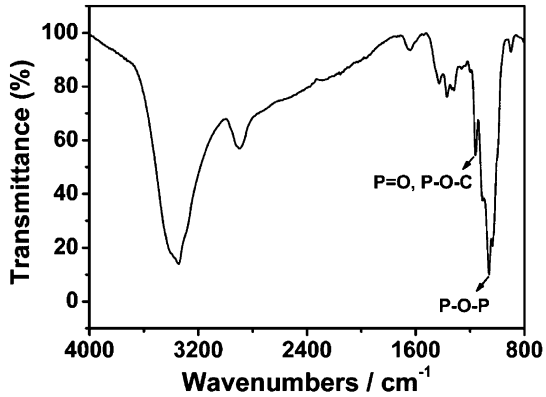

Figure 3. FTIR spectrum of the C2HC-700 sample.

composites are tested for supercapacitor applications. The effects of phosphate functionalization and CNT incorporation are investigated using multiple electrochemical techniques to obtain electrode materials with high performance.

2. EXPERIMENTAL SECTION

2.1. Synthesis of Carbon Composites. The phosphate-functionalized CNT-containing carbon composites were synthesized by one-pot soft-template hydrothermal method followed by further heat treatment at different temperatures under nitrogen atmosphere. For a typical run, 4 g of P123 and 2 mL of phosphoric acid were added into 68 mL of deionized water under constant stirring until P123 was dissolved. Then, 50 mg of CNTs (length, 1−2 μm; diameter, 10−20 nm) was dispersed in the P123 solution under ultrasound treatment for 2 h, and then 10 mL of saccharide solution containing 3 g of fructose was added to the CNT dispersion with an additional ultrasonic treatment for 30 min. The mixture was then transferred to a Teflon autoclave, sealed, and treated at 120 °C for 24 h. The product was separated and dried at 80 °C, followed by further heat treatment at 700 °C under nitrogen atmosphere. A series of samples containing different amounts of CNTs were synthesized by adding 0, 5, 50, and 100 mg of CNTs, which was denoted as C*x*HC-700 (*x* = 0, 1, 2, 3 corresponding to different additive amounts of CNTs). The C2HC

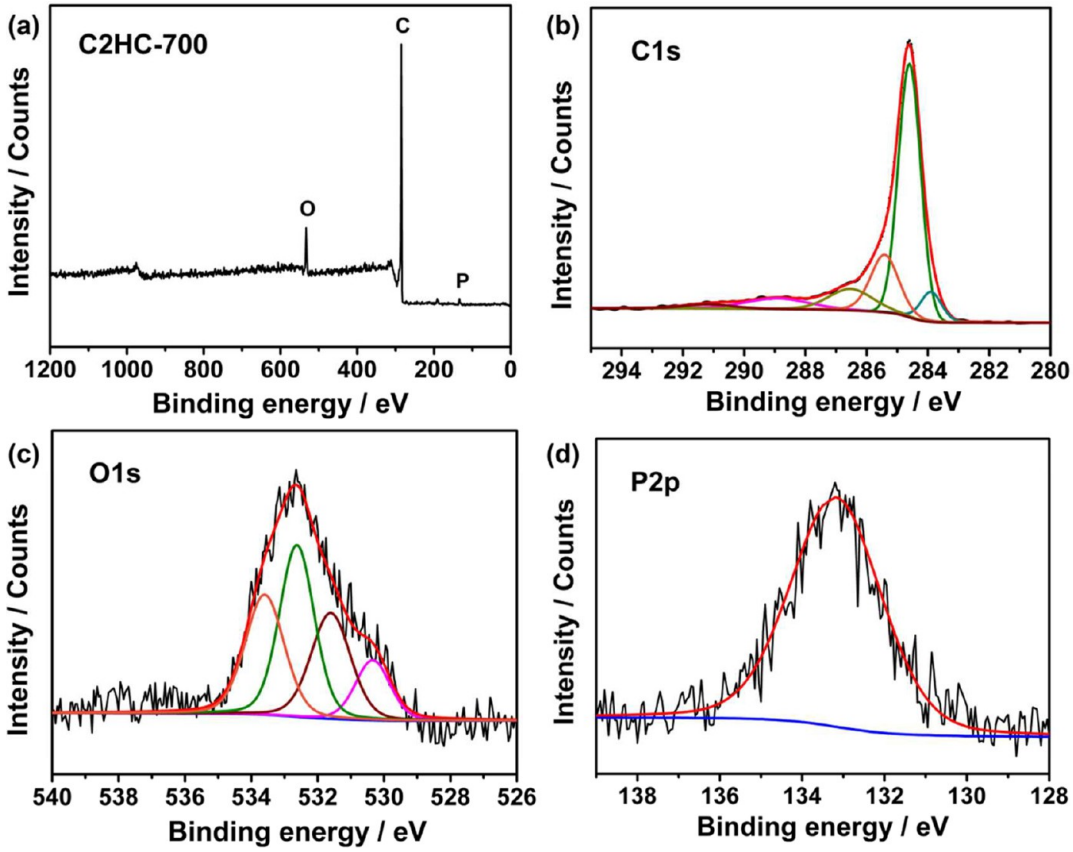

Figure 4. (a) XPS survey spectrum of the C2HC-700 sample and deconvoluted high-resolution (b) C1s, (c) O1s, and (d) P2p spectra of the C2HC-700 sample.

Table 2. Deconvolution Results of XPS Spectra of the C2HC-700 Sample

region	content (at %)	position (eV)	assignment	percentage (%)[a]
C1s	89.6	283.9	carbide	6.8
		284.6	graphite	55.7
		285.4	R−OH + C−O−C + C−O−P	17.5
		286.5	C═O + >C═O	10.3
		288.9	COOH + −C(O)−O−C	7.5
		291.2	$\pi-\pi^*$	2.2
O1s	8.0	530.3	quinones	12.3
		531.6	=O	24.7
		532.6	−O−	35.4
		533.6	OH	27.6
P2p	2.5	133.2	phosphates and pyrophosphates	100

[a]Relative percentage of each component deconvoluted from the high-resolution XPS spectra of C1s, O1s, and P2p.

sample was also heated at 800 and 900 °C under nitrogen atmosphere to yield C2HC-800 and C2HC-900 samples.

2.2. Characterizations. Morphologies and microstructures of carbon composites were examined by a field emission scanning electron microscopy (FE-SEM, FEI NOVA NanoSEM 450, operated at 3 kV) and a transmission electron microscopy (TEM, Philips Tecnai G220, operated at 120 kV). Specific surface area and pore size distribution were calculated based on the nitrogen physical sorption (Micromeritics ASAP 2020). The composites were degassed at 200 °C for 5 h prior to the nitrogen sorption measurement. A Fourier transform infrared (FTIR) microspectroscopy (Thermo Scientific Nicolet iN10) was used to investigate to surface properties. Thermogravimetric analysis (TGA, Mettler Toledo 851e) was conducted in air from room temperature to 850 °C at a rate of 10 °C min^{-1}. The X-ray photoelectron spectroscopy (XPS, Thermo ESCALAB 250) measurement was performed to analyze the surface properties quantitatively. The electrical conductivities were calculated according the results measured by the four-probe method using a S-2A four-probe station and Keithley 2400 Sourcemeter.

2.3. Electrochemical Measurements. The cyclic voltammetry, galvanostatic charge−discharge, electrochemical impedance spectroscopy (EIS) and galvanostatic cycling test were carried out using CHI 660D (Shanghai Chenhua, China) electrochemical workstation in a three-electrode cell with 6 M KOH as electrolyte solution. Active materials and binder poly(tetrafluoroethylene) with a mass ratio of 95:5 were pressed onto the nickel foam that were used as the work electrode. Hg/HgO electrode and Pt foil electrode were used as reference electrode and counter electrode in the three-electrode cell, respectively. Cyclic voltammetry and galvanostatic cycling stability test were also carried out in the two-electrode cell assembled by two symmetrical work electrode at different cell voltages. The cell was operated at cell voltage of 0.9 V for the first 5000 cycles followed by another 5000 cycles at a cell voltage of 1.2 V and a current density of 5 A g^{-1} for cycling test.

3. RESULTS AND DISCUSSION

Functional carbon composites with hierarchical porous structure were prepared by a simple one-pot soft-template hydrothermal reaction of copolymer, CNTs, fructose, and H_3PO_4 followed by heat treatment. In this approach, as shown in Scheme 1, triblock copolymer Pluronic P123 has dual functions, i.e., to help disperse CNTs uniformly and serve as mesopore template where carbonaceous sol intermediates

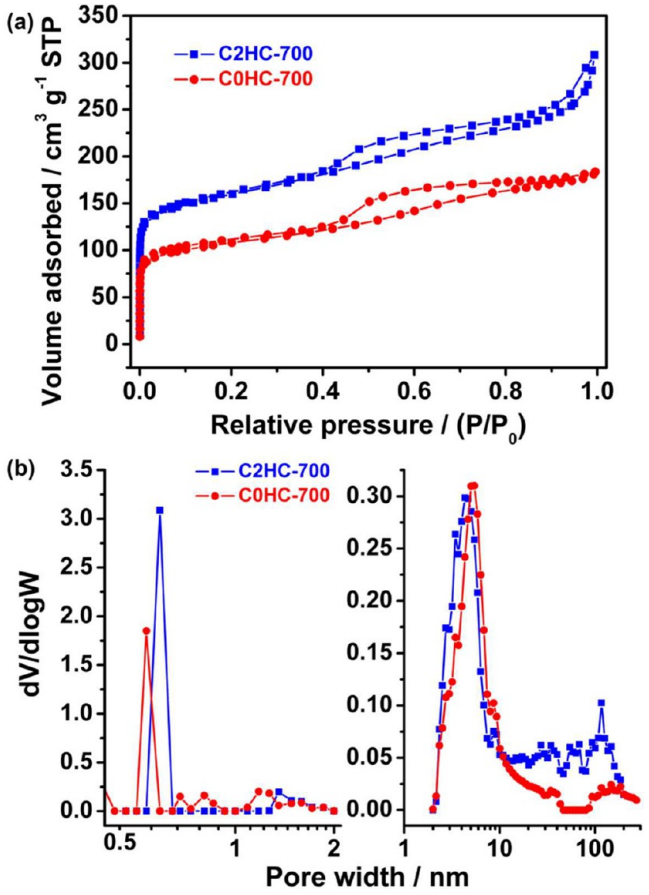

Figure 5. (a) Nitrogen adsorption−desorption isotherms and (b) pore-size distributions of the C0HC-700 and C2HC-700 samples.

originated from fructose in the hydrothermal process can assemble in situ. The phosphate-functionalized CNT-containing carbon composites termed as C*x*HC-T were obtained by heating the precursor C*x*HC at different temperatures.

Figure 1 shows the typical FE-SEM and TEM images of a series of carbon composites containing different amounts of CNTs. In the sample without CNTs, amorphous bulk carbon particles can be clearly seen, as shown in Figure 1a. For the carbon composites with CNTs, as shown in Figure 1b-d, CNTs are well-dispersed in the carbon matrix, and no obvious differences are observed though the CNT content varies in the composites. Further TEM examination (see Figure 1e, f) reveals that the wormlike disordered mesopores with a diameter of 3−5 nm are present in the C0HC-700 and C2HC-700 samples, where CNTs are uniformly embedded in the mesoporous carbon matrix (Figure 1f and Figure S3 in the Supporting Information). It is believed that the wormhole mesopores are formed because of the self-assembly interaction between P123 micelles and carbonaceous sol intermediates generated in the hydrothermal step followed by heat treatment. The uniform dispersion of CNTs in the carbon matrix is due to the hydrophobic−hydrophobic interaction between P123 and CNTs that results in the uniform dispersion of CNTs in water under ultrasonic treatment (see Figure S1 in the Supporting Information). The actual content of CNTs in the carbon composites was obtained by thermogravimetric analysis, the results of which are shown in Figure 2 and Table S1 in the Supporting Information. The calculated content of CNTs in the C0HC-700, C1HC-700, C2HC-700, and C3HC-700 samples is 0, 1.3, 9.3, and 15.3%, respectively. With increasing the content of CNTs, the electrical conductivity of the carbon composites also increases because of the high conductivity of CNTs, and the results are shown in Table 1.

The FTIR microspectroscopy study confirms that the phosphate groups are present in the composites, as can be seen in Figure 3. The spectrum shows typical characteristic of phosphocarbonaceous compounds present in the carbons materials activated by phosphoric acid. The peak at 1160 cm^{-1} is due to the stretching vibration of hydrogen-bonded P═O groups and the O−C stretching vibration in the P−O−$C_{aromatic}$ linkage, and the peak at 1062 cm^{-1} is assigned to the symmetrical vibration in polyphosphate chain P−O−P.[21] The XPS spectra of the C2HC-700 sample were also collected to further analyze the surface chemistry properties of the carbon composite. The spectrum in Figure 4a indicates the presence of phosphorus species in the composite and the phosphorus content is 2.5 at%. High-resolution XPS spectrum of P2p peak can be deconvoluted into the peak with a binding energy at 133.2 eV, which can be identified as the phosphorus species as tetra-coordinated phosphorus(V) (Table 2).[22,23] The spectra of C1s peak and O1s peak can be deconvoluted into six components and four components, respectively, and the results were summarized in Table 2. The carbon species correspond to carbide carbon (283.9 eV); graphite carbon (284.6 eV); carbon in alcohol, ether groups, and/or C−O−P linkage (285.4 eV); carbon in carbonyl groups (286.5 eV); carboxyl and/or ester groups (288.9 eV); and $\pi-\pi^*$ transitions in aromatic rings (291.2 eV).[22] The oxygen species represent quinones (530.3 eV); oxygen double-bonded to carbon (C═O) and non-bridging oxygen in the phosphate groups (P═O) (531.6 eV); oxygen single-bonded to carbon in C−O and in C−O−P groups (532.6 eV); and oxygen single bonds in hydroxyl groups (533.6 eV).[22,24]

The porosity of the as-made carbon materials was analyzed by N_2 adsorption technique. Figure 5a is the isotherms of the C0HC-700 and C2HC-700 samples, showing a combined characteristic of type I/IV isotherms. For the C0HC-700 sample, its BET surface area is 392 m^2 g^{-1}. For the C2HC-700 sample, its BET surface area is 587 m^2 g^{-1}. The pore size distribution of the C2HC-700 sample shows a similar hierarchical porous structure in comparison to C0HC-700 in the region of 0.5 to 10 nm, of which the difference is that C2HC-700 contains more larger mesopores (20−50 nm) and macropores (50−200 nm), as shown in Figure 5b. The average micropore size of C0HC-700 is 0.54 nm, which is smaller than 0.59 nm of C2HC-700. The formation of micropores is possibly due to the activation by H_3PO_4 in the post heat treatment step. Besides, the mesopores in the C0HC-700 and C2HC-700 samples formed by the soft template P123 are 4.4 and 5.2 nm, respectively, and this is consistent with the TEM results (Figure 1e, f). This will demonstrate that the hierarchical pore structures have been formed in the composites. Interestingly, the large mesopores and macropores in the C2HC-700 sample are due to the presence of CNTs (see Figure S2 in the Supporting Information), which can function as a fast ion-transport pathway that further improve the rate capability of the supercapacitors.[7]

To evaluate the effect of CNT on the electrochemical performance of the C*x*HC-700 samples, cyclic voltammetry, galvanostatic charge−discharge, and electrochemical impedance spectroscopy (EIS) were recorded in 6 M KOH aqueous solution in a three-electrode cell. Figure 6a, b show the cyclic

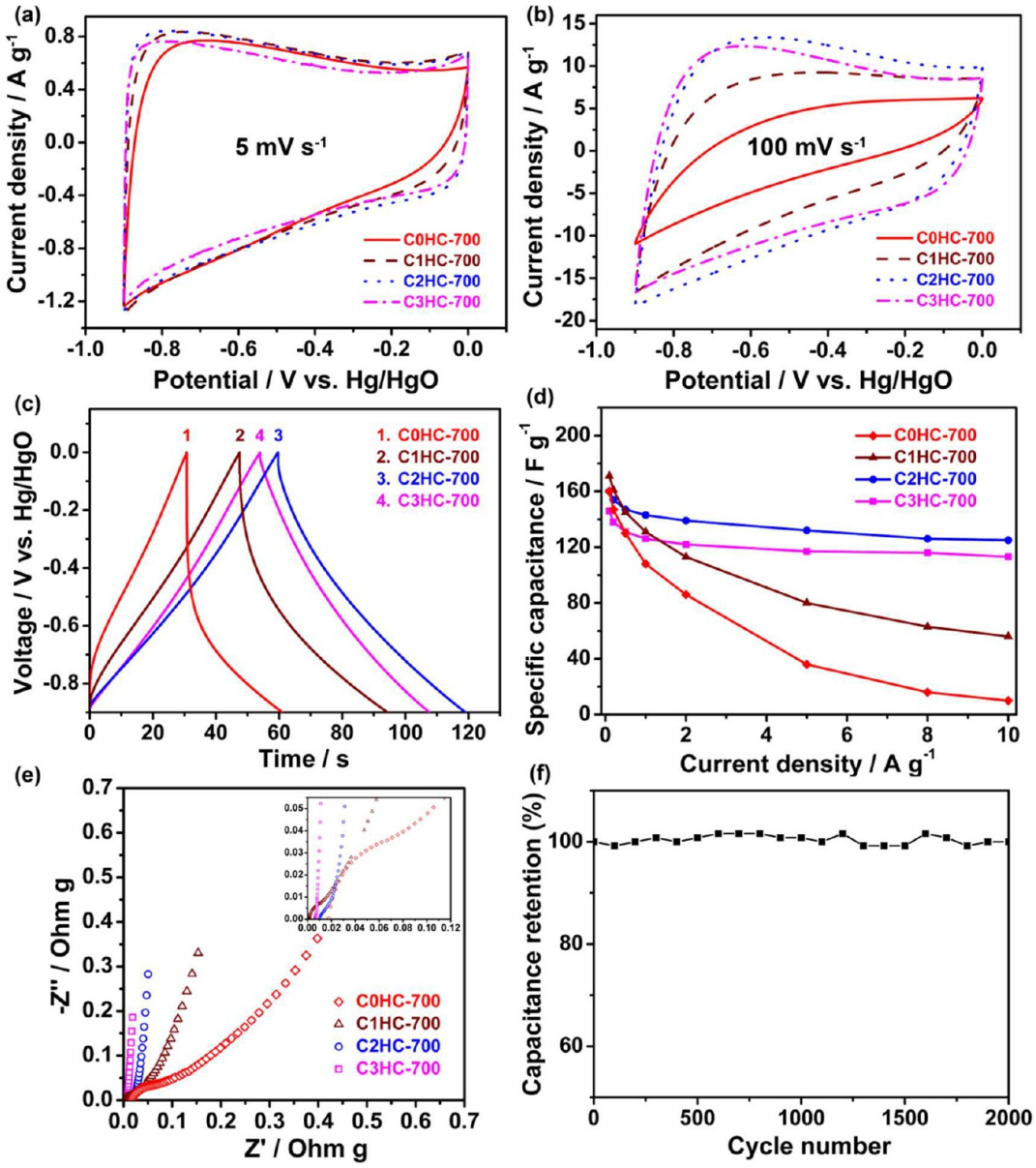

Figure 6. Cyclic voltammograms recorded at (a) 5 mV s^{-1} and (b) 100 mV s^{-1}. (c) Galvanostatic charge−discharge curves at 2 A g^{-1}. (d) Specific capacitances at different current densities. (e) Nyquist plots of the carbon composites heated at 700 °C. (f) Galvanostatic cycling test of C2HC-700 at a current density of 5 A g^{-1}.

voltammetry (CV) curves of the samples at a scan rate of 5 and 100 mV s^{-1}, respectively. The CV curves for all of the samples show good rectangular shapes at 5 mV s^{-1} (Figure 6a), for C2HC-700 and C3HC-700 with a higher CNT content, a faster electrochemical response is observed, evidencing a better ideal electrical double layer capacitor (EDLC) behavior. At higher scan rate of 100 mV s^{-1} (Figure 6b), the CV curve for the hydrothermal carbon C0HC-700 without CNTs shows a completely distorted rectangular shape, in the case of C1HC-700 with a CNT content of 1.3 wt %, the shape of CV curve is improved to some degree. As the CNT content further increases, the CV curves for the C2HC-700 and C3HC-700 with a higher CNT content display relatively good rectangular shape at the high scan rate, implying that the presence of CNTs dispersed in the carbon matrix can obviously enhance the rate capability of carbon composites.

Figure 6c shows the galvanostatic charge−discharge curves of CxHC-700 at a current density of 2 A g^{-1}. In comparison with the C0HC-700 and C1HC-700 samples, the C2HC-700 and C3HC-700 samples show better linear characteristics, indicating that the composites containing more CNTs have a better reversible charge−discharge property. This is in consistent with the cyclic voltammetry results. The relationship between the specific capacitance and the current density is also observed in Figure 6d according to the galvanostatic charge and discharge results collected at different current densities. At a current density from 0.1 to 10 A g^{-1}, the C2HC-700 and C3HC-700 samples with higher CNT content show higher capacitance retention. Even at a high current density of 10 A g^{-1}, the specific capacitances of C2HC-700 and C3HC-700 can remain 78.1% (125 F g^{-1}) and 77.4% (113 F g^{-1}) with the capacity at 0.1 A g^{-1} as reference, under the identical conditions, the specific capacitances of C0HC-700 and C1HC-700 only remain 6.3 and 32.7%. The Nyquist plots of C2HC-700 and C3HC-700 with higher CNT contents shown in Figure 6e exhibit a lower charge transfer resistance and a better capacitive

dx.doi.org/10.1021/am303052n | ACS Appl. Mater. Interfaces 2013, 5, 2104−2110

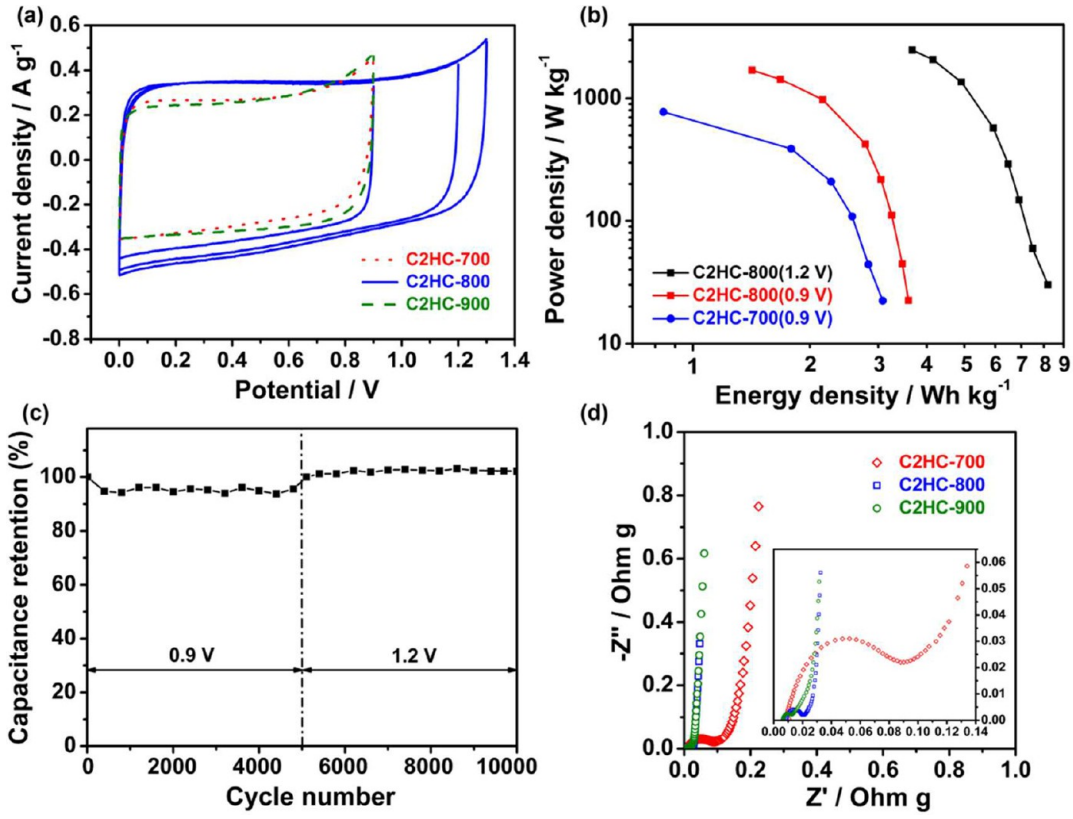

Figure 7. (a) Cyclic voltammograms of C2HC-700, C2HC-800, and C2HC-900 at 5 mV s^{-1} and the cell voltage of 0.9, 1.2, and 1.3 V. (b) Regone plots of C2HC-700 obtained at 0.9 V and C2HC-800 obtained at 0.9 and 1.2 V. (c) Galvanostatic cycling test of C2HC-800 at 5 A g^{-1} and the cell voltage of 0.9 and 1.2 V. (d) Nyquist plots of C2HC-700, C2HC-800, and C2HC-900.

behavior. Moreover, the C2HC-700 also shows good cycling stability at a high current of 5 A g^{-1}, without any loss in the initial capacity even after 2000 cycles, as shown in Figure 6f. These improved performance is due to the CNTs dispersed in the carbon matrix that help create large mesopores and macropores for fast ion transport, and improve the mechanical property and electrical conductivity of the carbon composites. These combined effects bring about the improvements in the rate capability and cycle stability at high current load.[7,15]

The electrochemical capacitive behaviors of the C2HC-T treated at different temperatures were also examined. It has been found that a wider operating cell voltage window can be achieved by simply increasing the heat treatment temperature from 700 to 800 °C, as can be seen in Figure 7. The CV curve of the C2HC-800 sample exhibits an ideal rectangular shape at a cell voltage of 0.9 V, indicating that C2HC-800 has an ideal EDLC behavior, while the C2HC-700 and C2HC-900 cannot withstand at the same cell voltage, which is evidenced by the electrolyte decomposition peaks (Figure 7a). Moreover, C2HC-800 also demonstrates stable EDLC performance even at higher cell voltage up to 1.2 V, which is very close to the theoretical decomposition potential of water (1.23 V), and the electrolyte decomposition peak seems to appear at a cell voltage of 1.3 V. The wider operating voltage window is believed to be due to the highest phosphate groups content in C2HC-800, which is similar to the results reported in the literatures.[21,22] The phosphate groups can block the nonstable active oxidation sites.[11] Widening the operating voltage up to 1.2 V can significantly increase the energy density of the devices since it is proportional to the square of the cell voltage. Regone plots of C2HC-700 obtained at 0.9 V and C2HC-800 obtained at 0.9 and 1.2 V are shown in Figure 7b. The specific energy density of the two-electrode cell constructed of C2HC-800 at 1.2 V increases to 8.2 W h kg^{-1}, whereas the specific power density is 30 W kg^{-1}.

The C2HC-800 also shows extraordinary electrochemical cycling stability while galvanostatic charging and discharging at a wide cell voltage of 1.2 V and a high current density of 5 A g^{-1}, as can be seen in Figure 7c. The reason for this is partly due to the fact that the heat treatment at higher temperature significantly decreases the equivalent series resistance and the charge transfer resistance to a degree (Figure 7d). The prolonged cycling stability at high current load reported here is also due to the combined effect of CNTs that helps enhance the mechanical stability of CNT/carbon composites during charging and discharging.[15]

4. CONCLUSIONS

In conclusion, phosphate-functionalized CNT-containing carbon composites with hierarchical porous structure have been prepared by an one-pot soft-template hydrothermal reaction of copolymer, CNTs, fructose, and H_3PO_4 followed by heat treatment. CNTs networks embedded in the carbon matrix improve the rate capability of carbon composites. Furthermore, the phosphate groups and CNTs jointly contribute to the high rate performance of carbon composites that have highly stable cycling performance at wide cell voltage of 1.2 V and high current load of 5 A g^{-1}.

■ ASSOCIATED CONTENT

Ⓢ Supporting Information

The optical photograph of P123-assisted CNTs dispersion. Nitrogen adsorption−desorption isotherms and pore size

distribution of CNTs. TEM images of the C2HC-700 sample. Volumetric specific capacitances and energy densities of the samples. Table that summarizes the compositions and properties of the as-prepared samples. This material is available free of charge via the Internet at http://pubs.acs.org/.

AUTHOR INFORMATION

Corresponding Author

*Address: No. 2 Linggong Road, High Technology Zone, Dalian City, Liaoning Province, China. E-mail: jqiu@dlut.edu.cn. Tel: +86-411-84986024. Fax: +86-411-84986080.

Notes

The authors declare no competing financial interest.

ACKNOWLEDGMENTS

This work was partly supported by the National Natural Science Foundation of China (50902016, 20923006, and U1203292) and Dalian Municipal Science & Technology Project of China (2011A15GX023).

REFERENCES

(1) Ghosh, A.; Lee, Y. H. *ChemSusChem* **2012**, *5*, 480−499.
(2) Zhai, Y.; Dou, Y.; Zhao, D.; Fulvio, P. F.; Mayes, R. T.; Dai, S. *Adv. Mater.* **2011**, *23*, 4828−4850.
(3) Chmiola, J.; Yushin, G.; Gogotsi, Y.; Portet, C.; Simon, P.; Taberna, P. L. *Science* **2006**, *313*, 1760−1763.
(4) Wang, D.-W.; Li, F.; Liu, M.; Lu, G. Q.; Cheng, H.-M. *Angew. Chem., Int. Ed.* **2008**, *47*, 373−376.
(5) Hulicova-Jurcakova, D.; Seredych, M.; Lu, G. Q.; Bandosz, T. J. *Adv. Funct. Mater.* **2009**, *19*, 438−447.
(6) Wu, Z.-S.; Winter, A.; Chen, L.; Sun, Y.; Turchanin, A.; Feng, X.; Müllen, K. *Adv. Mater.* **2012**, *24*, 5130−5135.
(7) Raymundo-Piñero, E.; Cadek, M.; Wachtler, M.; Béguin, F. *ChemSusChem* **2011**, *4*, 943−949.
(8) Chen, Y.; Zhang, X.; Zhang, H.; Sun, X.; Zhang, D.; Ma, Y. *RSC Adv.* **2012**, *2*, 7747−7753.
(9) Wang, Y.-G.; Li, H.-Q.; Xia, Y.-Y. *Adv. Mater.* **2006**, *18*, 2619−2623.
(10) Subramanian, V.; Zhu, H.; Wei, B. *Electrochem. Commun.* **2006**, *8*, 827−832.
(11) Hulicova-Jurcakova, D.; Puziy, A. M.; Poddubnaya, O. I.; Suárez-García, F.; Tascón, J. M. D.; Lu, G. Q. *J. Am. Chem. Soc.* **2009**, *131*, 5026−5027.
(12) Fulvio, P. F.; Mayes, R. T.; Wang, X.; Mahurin, S. M.; Bauer, J. C.; Presser, V.; McDonough, J.; Gogotsi, Y.; Dai, S. *Adv. Funct. Mater.* **2011**, *21*, 2208−2215.
(13) Portet, C.; Yushin, G.; Gogotsi, Y. *Carbon* **2007**, *45*, 2511−2518.
(14) Shen, J.; Liu, A.; Tu, Y.; Foo, G.; Yeo, C.; Chan-Park, M. B.; Jiang, R.; Chen, Y. *Energ. Environ. Sci.* **2011**, *4*, 4220−4229.
(15) Noked, M.; Okashy, S.; Zimrin, T.; Aurbach, D. *Angew. Chem., Int. Ed.* **2012**, *51*, 1568−1571.
(16) Hu, B.; Wang, K.; Wu, L.; Yu, S.-H.; Antonietti, M.; Titirici, M.-M. *Adv. Mater.* **2010**, *22*, 813−828.
(17) Kubo, S.; White, R. J.; Yoshizawa, N.; Antonietti, M.; Titirici, M.-M. *Chem. Mater.* **2011**, *23*, 4882−4885.
(18) Zhu, H.; Wang, X.; Yang, F.; Yang, X. *Adv. Mater.* **2011**, *23*, 2745−2748.
(19) Zhao, L.; Fan, L.-Z.; Zhou, M.-Q.; Guan, H.; Qiao, S.; Antonietti, M.; Titirici, M.-M. *Adv. Mater.* **2010**, *22*, 5202−5206.
(20) Titirici, M.-M.; White, R. J.; Falco, C.; Sevilla, M. *Energ. Environ. Sci.* **2012**, *5*, 6796−6822.
(21) Puziy, A. M.; Poddubnaya, O. I.; Martínez-Alonso, A.; Castro-Muñiz, A.; Suárez-García, F.; Tascón, J. M. D. *Carbon* **2007**, *45*, 1941−1950.
(22) Puziy, A. M.; Poddubnaya, O. I.; Socha, R. P.; Gurgul, J.; Wisniewski, M. *Carbon* **2008**, *46*, 2113−2123.
(23) Carriazo, D.; Gutierrez, M. C.; Pico, F.; Rojo, J. M.; Fierro, J. L.; Ferrer, M. L.; Del Monte, F. *ChemSusChem* **2012**, *5*, 1405−1409.
(24) Arrigo, R.; vecker, M. H.; Wrabetz, S.; Blume, R.; Lerch, M.; McGregor, J.; Parrott, E. P. J.; Zeitler, J. A.; Gladden, L. F.; Knop-Gericke, A.; Schlögl, R.; Su, D. S. *J. Am. Chem. Soc.* **2010**, *132*, 9616−9630.